HHS Public Access

Author manuscript

J Biol Inorg Chem. Author manuscript; available in PMC 2016 July 01.

Published in final edited form as:

J Biol Inorg Chem. 2015 July ; 20(5): 805–819. doi:10.1007/s00775-015-1267-1.

The Response of Ω-Loop D Dynamics to Truncation of Trimethyllysine 72 of Yeast Iso-1-cytochrome *c* Depends on the Nature of Loop Deformation

Levi J. McClelland, **Sean M. Seagraves, Md.**, **Khurshid Alam Khan**[†], **Melisa M. Cherney**[‡], **Swati Bandi**[§], **Justin E. Culbertson**, and **Bruce E. Bowler**

Department of Chemistry & Biochemistry, Center for Biomolecular Structure and Dynamics, University of Montana, Missoula, Montana 59812

Abstract

Trimethyllysine 72 (tmK72) has been suggested to play a role in sterically constraining the heme crevice dynamics of yeast iso-1-cytochrome *c* mediated by the Ω-loop D cooperative substructure (residues 70 to 85). A tmK72A mutation causes a gain in peroxidase activity, a function of cytochrome *c* that is important early in apoptosis. More than one higher energy state is accessible for the Ω-loop D substructure via tier 0 dynamics. Two of these are alkaline conformers mediated by Lys73 and Lys79. In the current work, the effect of the tmK72A mutation on the thermodynamic and kinetic properties of wild type iso-1-cytochrome *c* (yWT versus WT*) and on variants carrying a K73H mutation (yWT/K73H versus WT*/K73H) is studied. Whereas the tmK72A mutation confers increased peroxidase activity in wild type yeast iso-1-cytochrome *c* and increased dynamics for formation of a previously studied His79-heme alkaline conformer, the tmK72A mutation speeds return of the His73-heme alkaline conformer to the native state through destabilization of the His73-heme alkaline conformer relative to the native conformer. These opposing behaviors demonstrate that the response of the dynamics of a protein substructure to mutation depends on the nature of the perturbation to the substructure. For a protein substructure which mediates more than one function of a protein through multiple non-native structures, a mutation could change the partitioning between these functions. The current results suggest that the tier 0 dynamics of Ω-loop D that mediates peroxidase activity has similarities to the tier 0 dynamics required to form the His79-heme alkaline conformer.

Keywords

Cooperative substructure dynamics; Cytochrome *c*; Alkaline conformational transition; Conformationally-gated electron transfer

Tel: (406) 243-6114. Fax: (406) 243-4227. bruce.bowler@umontana.edu.

[†]Present address: School of Life Sciences, B.S. Abdur Rahman University, GST Road, Vandalur, Chennai, 600048, India

[‡]Present address: Department of Chemistry and Biochemistry, University of Northern Iowa, Cedar Falls, Iowa 50614

[§]Present address: Department of Pharmaceutical Sciences, University of Colorado School of Pharmacy, Aurora, Colorado 80045

Introduction

Tier 0 dynamics, which involves interconverison between conformers separated by a thermal barrier, is particularly important in protein function, often controlling access to functionally active conformers [1]. A detailed understanding of the structural factors that control tier 0 dynamics and thus the function of proteins is essential. Cytochrome *c* (Cyt*c*) has long been a protein of interest due to both its function in electron transport [2] and its role in apoptosis [3]. Of particular interest with regard to these functions are the heme crevice dynamics, which can be studied with the alkaline conformational transition of Cyt*c* [4]. The alkaline conformational transition is an example of tier 0 dynamics because the barrier between the native and alkaline states is significantly larger than ambient thermal energy [1, 5].

Here, we use yeast iso-1-cytochrome *c* (iso-1-Cyt*c*) as a vehicle to probe the structural factors controlling protein dynamics. Residues 70-85 of iso-1-Cyt*c* comprise the heme crevice loop, Ω-loop D (Fig. 1), which lies across one face of the heme. These residues are highly conserved across Cyt*c* from different species [2, 6]. Met80 is bound to the sixth coordination site of the heme in the native iso-1-Cyt*c* conformer [7]. During the tier 0 alkaline conformational transition of the ferric state of Cyt*c*, the Met80-heme ligand is replaced by lysine residues within Ω-loop D. These conformational changes are of particular biological interest because replacement of Met80-heme ligation with Lys-heme ligation can modulate electron transfer properties, possibly optimizing electron flow in the Electron Transport chain [4, 8-12]. The Met80 ligand must also leave the 6^{th} coordination site of the heme in order for peroxidase activity to occur in the beginning stages of apoptosis [3]. Apoptosis can be induced in yeast, causing release of Cyt*c* from the mitochondria. However, the proteins needed to form an apoptosome in the cytoplasm and induce the caspase cascade, which leads to cell death in higher eukaryotes, are missing [16]. Given the high degree of conservation of Ω-loop D in Cyt*c* (13 of 16 residues are conserved from yeast to mammals, [2, 6]), studies on the dynamics of this loop in iso-1-Cyt*c* provide a relevant model for heme crevice dynamics as it relates to peroxidase activity early in apoptosis, prior to release of cytochrome *c* from the mitochondria.

An increase in pH triggers ionization events leading to replacement of the native state Met80-heme ligand by either Lys73 or Lys79 in the alkaline conformational transition [17, 18]. The alkaline conformational transition of wild-type iso-1-Cyt*c* expressed from yeast (yWT) is a monophasic conformational transition with either Lys73 or Lys79 replacing Met80 with similar, but not identical, kinetics and thermodynamics [18, 19]. Variants with a Lys73 to histidine mutation exhibit a biphasic alkaline transition where His73-heme ligation occurs near neutral pH, followed by Lys79-heme ligation above pH 8 [9, 20-22]. Not only does incorporating His into Ω-loop D enable the distinction between residues replacing Met80, but additionally the shift in the apparent pK_a, pK_{app}, of the alkaline transition allows the conformational change to be monitored more effectively because it can be done near neutral pH [20, 23]. Thus, characterization of the dynamics of His-heme conformers allows for thorough investigation of the effect of point mutations on Cyt*c* dynamics as it relates to function.

In yWT iso-1-Cyt*c*, the lysine at residue 72 undergoes posttranslational modification to trimethyllysine (tmK). During expression from *Escherichia coli* Lys72 is not trimethylated. Lack of trimethylation allows Lys72 to become a heme ligand in the alkaline conformational transition [24]. In order to prevent Lys72-heme ligation during the alkaline conformational transition, residue 72 can be mutated to alanine [24]. Analysis of the native conformer of yeast iso-1-Cyt*c* (pdb code: 2YCC), shows that loss of a lysine residue at position 72 also results in a loss of contacts between residue 72 and residues Thr78, Met80 and Ala81 on the opposite side of Ω-loop D (Fig. 1) [7]. We have recently reported the crystal structure of tmK72A iso-1-Cyt*c*, which indicates that reducing the steric size of the residue at position 72 favors formation of an alternate conformer with hydroxide replacing Met80 as the heme ligand near pH 9 [25]. Also, we have previously reported increased heme crevice dynamics for the His79-heme alkaline conformational transition for a K79H variant with a tmK72A mutation compared to yWT/K79H iso-1-Cyt*c* which contains tmK72 [26, 27]. For horse Cyt*c*, spin-labeling of Lys72 demonstrates that this residue is relatively immobile suggesting that the residue at this position may be important for modulating the dynamics of Ω-loop D in Cyt*c* across a broad range of species [28]. Furthermore, the tmK72A mutation leads to enhanced peroxidase activity for iso-1-Cyt*c* [25]. Thus, the residue at position 72 may modulate the dynamics of Ω-loop D necessary for peroxidase activity.

Both residues 73 and 79 belong to Ω-loop D, which is the second least stable of five cooperative substructures (see Fig. 1), which have been identified in Cyt*c* using native state H/D exchange methods [13-15]. Although both residues 73 and 79 belong to the same cooperative substructure of Cyt*c*, it is unclear whether dynamics mediated by deformation of a cooperative substructure from two different points in the substructure will be affected in the same way by a point mutation. Greater understanding of the dynamics of cooperative substructures is important for understanding how tier 0 dynamics affect protein function, in general. In the case of Cyt*c*, the effect of the tmK72A mutation on Ω-loop D mediated from position 73 versus 79 could provide greater insight into the nature of the dynamics required for peroxidase function at the onset of apoptosis. Previous work has shown that the mechanisms of the His79-mediated alkaline transition and the His73-mediated alkaline transition differ [9, 21-23, 26, 27, 29, 30]. Additionally, denaturant *m*-values, which correlate to the surface area exposed by partial or full unfolding of a protein [15, 31, 32], are smaller for formation of the His79-heme alkaline conformer than for the His73-heme alkaline conformer indicating less structural rearrangement during formation of the His79-heme conformer than for the His73-heme conformer [20, 22, 23, 33]. Similarly, the enthalpies of the alkaline transition mediated by Lys73 versus Lys79, also differ significantly [18]. These differences between both the kinetic and thermodynamic properties of alkaline transitions of Cyt*c* mediated by two different sequence positions along the Ω-loop D substructure, suggest that the effects of the tmK72A mutation on the dynamics of a K73H variant of iso-1-Cyt*c* could differ from those of a K79H variant.

In order to investigate the effect of the tmK72A mutation on the dynamics of the His73-mediated versus His79-mediated alkaline transition, we have characterized the thermodynamic and kinetic properties of the His73-mediated alkaline conformational of tmK72A/K73H iso-1-Cyt*c* allowing comparison with previous work on K73H variants of

iso-1-Cyt*c*. The data show that the His73-mediated alkaline transition is less favorable in the presence of the tmK72A mutation and that the dynamics of return to the native state from the His73-heme alkaline conformer are increased. This result contrasts markedly with the increase in stability of the His79-heme alkaline conformer relative to the native state of iso-1-Cyt*c* and the increase in the dynamics of formation of the His79-heme alkaline conformer upon introduction of the tmK72A mutation [26, 27].

Materials and methods

Preparation of iso-1-Cyt*c* variants

Two variants of iso-1-Cyt*c* were used in this work: WT*, which contains C102S and K72A mutations and WT*/K73H, which adds the K73H mutation to the WT* background. The C102S mutation prevents disulfide dimerization during physical studies. The K72A mutation is commonly used in *Escherichia coli*-expressed iso-1-Cyt*c* to prevent Lys72, which is trimethylated in its native host, *Saccharomyces cerevisiae*, from acting as an alkaline state ligand [24]. Both proteins were expressed from the pRbs_BTR1 vector [34], which is a derivative of the pBTR1 vector [24, 35] with an optimized ribosomal binding site [36]. This vector co-expresses the iso-1-Cyt*c* (*CYC1*) and the heme lyase (*CYC3*) genes from *S. cerevisiae*, so that heme insertion occurs efficiently in the cytoplasm of *E. coli*. The pRbs_BTR1 vector was originally prepared carrying the TM variant (H26N, H33N, H39Q, C102S) of iso-1-Cyt*c* [34]. Conversion to the WT* variant was accomplished in four steps. A K72A mutation was first introduced into this vector using the unique restriction site elimination method [37] with single-stranded pRbs_BTR1 DNA as template. The K72A oligonucleotide and the selection primer $EcoRV^{-}AatII^{+}$ (see Table S1, eliminates a unique EcoRV site and creates a unique AatII site in pRbs_BTR1) were used to introduce the K72A mutation. The remaining mutations were introduced using double-stranded pRbs_ BTR1 DNA as template and the PCR-based QuikChange protocol (Agilent Technologies). The wild type histidines of iso-1-Cyt*c* were reintroduced into the *CYC1* gene in the order His26, His39 and His33 using the primer pairs, N26H and N26H-r, Q39H and Q39H-r, and N33H and N33H-r (Table S1), respectively. The pRbs_BTR1 vector containing the WT* variant was used as the template to prepare the WT*/K73H variant with the QuikChange protocol and the primer pair K73H and K73H-r (Table S1). Each mutation to the *CYC1* gene was confirmed using dideoxy sequencing of the entire coding region of the gene. All sequencing was carried out at the Murdock DNA Sequencing Facility at the University of Montana.

Protein expression and purification

Protein was expressed in BL21(DE3) *E. coli* cells from the pRbs_BTR1 vector carrying either WT* or WT*/K73H iso-1-Cyt*c*, as described previously [26, 34]. Protein was purified as previously reported [26, 38, 39]. Briefly, after breaking the cells with a French Pressure Cell (SLM Aminco), the lysate was cleared by centrifugation. Contaminants were precipitated by adjusting the lysate to 50% ammonium sulfate. After centrifugation, the supernatant was dialyzed against 12.5 mM sodium phosphate buffer, pH 7.2, 1 mM EDTA, 2 mM β-mercaptoethanol (β-ME). Iso-1-Cyt*c* was batch absorbed to CM-Sepharose Fast Flow resin equilibrated with 50 mM sodium phosphate buffer, pH 7.2, 1 mM EDTA and 2 mM β-ME, then protein was eluted with a linear gradient of 0-0.8 M NaCl in 50 mM sodium

phosphate buffer, pH 7.2, 1 mM EDTA and 2 mM β-ME. Aliquots of about 2 mg/mL protein were flash frozen in liquid nitrogen and stored at -80 °C. Thawed aliquots were purified by cation-exchange HPLC using an Agilent Technologies 1200 series HPLC with a BioRad UNO S6 Column (catalog no. 720-0023). After collection of the iso-1-Cyt*c* peak, samples were concentrated by ultrafiltration before oxidation with $K_3[Fe(CN)_6]$. A G25 Sephadex column was used to separate the oxidized protein from the oxidizing agent.

The molecular weight of the WT* and WT*/K73H variants were measured to be 12,592.9 ± 0.1 g/mol (expected, 12,595.1 g/mol) and 12,603.3 ± 0.7 g/mol (expected, 12,604.1 g/mol) using a Bruker microflex MALDI-ToF mass spectrometer. Protein Calibration Standard I (Bruker Part No. 206355) was used to calibrate the mass spectrometer with an enhanced cubic calibration routine.

Global stability measurements by guanidine hydrochloride denaturation

Stability measurements by guanidine hydrochloride (GdnHCl) denaturation at 25 °C and pH 7.5 in 20 mM Tris and 40 mM NaCl buffer were monitored, as previously described [22], using an Applied Photophysics Chirascan circular dichroism (CD) spectrometer coupled to a Hamilton MICROLAB 500 Titrator. The free energy of unfolding in the absence of denaturant, $\Delta G_u^{o\prime}(H_2O)$, and the *m*-value were extracted from nonlinear least squares fits (SigmaPlot v. 7.0) of the data employing a two-state model assuming a linear free energy relationship [40], as previously described [41]. In these fits, the native state baseline was assumed to be independent of GdnHCl concentration [41]. Parameters are the average and standard deviation of a minimum of three independent trials.

pH titrations to measure the alkaline conformational transition of iso-1-Cyt*c* variants

pH titrations were carried out at 22 ± 1 °C to monitor the alkaline conformational transition of each variant. Titrations were followed at 695 nm, as previously reported [42], in 100 mM NaCl using a Beckman Coulter DU 800 UV/Vis spectrophotometer. 600 μL of a 2x stock solution containing 400 μM oxidized protein in 200 mM NaCl was prepared. 400 μL of the 2x stock solution was combined with 400 μL of MilliQ water and the solution was mixed with a 1000 μL pipetman. pH was adjusted by adding equal volumes of the 2x stock solution and either NaOH or HCl solutions of appropriate concentration and measured with a Denver Instrument UB-10 pH/mV meter using an Accumet semimicro calomel pH probe (Fischer Scientific Cat. No. 13-620-293). Baseline corrections were made by subtracting the absorbance at 750 nm, A_{750}, from the absorbance at 695 nm, A_{695}, yielding $A_{695corr}$. Corrected molar extinction coefficients, $\varepsilon_{695corr}$, were then calculated from $A_{695corr}$ using concentration evaluated from absorbance at 570 nm and 580 nm near pH 5 [23] and the known molar extinction coefficients for these wavelengths [43].

The monophasic $\varepsilon_{695corr}$ versus pH data from the WT* iso-1-Cyt*c* variant were fit to Eq. 1,

$$\varepsilon_{695corr} = \frac{\varepsilon_N + \varepsilon_{alk} * 10^{n[pK_{app} - pH]}}{1 + 10^{n[pK_{app} - pH]}} \quad (1)$$

using nonlinear least squares methods (SigmaPlot v. 7.0). Eq. 1 is a modified form of the Henderson-Hasselbalch equation, which allows the numbers of protons, *n*, linked to the

conformational change to be evaluated from the fit [20]. In Eq. 1, ε_N is the corrected extinction coefficient of the native state Met80-heme conformer at 695 nm, ε_{alk} is the corrected extinction coefficient of either the Lys73- or Lys79-heme bound alkaline state conformer at 695 nm, and pK_{app} is the apparent acid dissociation constant for the alkaline conformational transition.

The biphasic $\varepsilon_{695corr}$ versus pH data from the WT*/K73H variant were fit to a model (Eq. 2) which includes the ionization triggers for formation of both the His73-heme and Lys79-heme

$$\varepsilon_{695corr} = \frac{\left\{\varepsilon_N + \varepsilon_{alk} * \left(\frac{10^{\left[-pK_{C1}(His)\right]}}{1+10^{[pK_a(His)-pH]}} + \frac{10^{\left[-pK_{C2}(Lys)\right]}}{1+10^{[pK_a(Lys)-pH]}}\right)\right\}}{\left\{1+\left(\frac{10^{\left[-pK_{C1}(His)\right]}}{1+10^{[pK_a(His)-pH]}} + \frac{10^{\left[-pK_{C2}(Lys)\right]}}{1+10^{[pK_a(Lys)-pH]}}\right)\right\}} \quad (2)$$

conformers [20]. In Eq. 2, pK_a(His) and pK_a(Lys) are the acid dissociation constants for the ionizing trigger groups corresponding to population of the His73-heme and Lys79-heme conformers, respectively. pK_{C1}(His) and pK_{C2}(Lys) are the equilibrium constants corresponding to replacement of the Met80-heme ligand by the fully deprotonated His73 and Lys79 ligands, respectively. pK_a(Lys) was set to 10.8 as previously determined for the conformational change to the Lys79-heme alkaline state conformer [18]. Reported parameters from fits to Eqs. 1 and 2 are the average and standard deviation of a minimum of three independent trials.

pH jump stopped-flow kinetic experiments

All stopped-flow mixing experiments were carried out at 25 °C using an Applied Photophysics SX20 stopped-flow spectrometer, as previously reported [23]. Both long (50 – 350 s) and short (1 s) time scale data acquisitions were monitored at 406 nm, collecting 5000 points logarithmically for each. Upward pH jump mixing experiments began with 20 μM protein in 0.1 M NaCl at pH 5 followed by 1:1 mixing with 20 mM buffer in 0.1 M NaCl to achieve the desired pH. Upward pH jump experiments were carried out in steps of 0.25 pH units over the pH range of 6 – 10 for WT*/K73H. Downward pH jump experiments were executed in the same way but began at pH 8.05 and ended at pH values ranging from 5.0 – 6.5 in steps of 0.25 pH units. Buffers used were as follows: acetic acid (pH 5-5.25), MES (pH 5.5-6.5), NaH_2PO_4 (pH 6.75-7.5), Tris (pH 7.75-8.75), and H_3BO_3 (pH 9-10). In all cases the effluent was collected and the actual pH after mixing was determined with a Denver Instrument UB-10 pH/mV meter using an Accumet semimicro calomel pH probe. A minimum of 5 and 8 trials were collected for long and short time scale data acquisitions, respectively, for each pH jump experiment.

Heme reduction by hexaammineruthenium(II) chloride followed by stopped-flow

Conformationally-gated electron transfer (gated ET) experiments were performed by following reduction of oxidized WT*/K73H Cyt*c* at 550 nm, a wavelength that is very sensitive to the redox state of Cyt*c*, with an Applied Photophysics SX20 stopped-flow spectrometer using previously established methods [9, 23, 29, 44]. The reducing reagent,

hexaammineruthenium(II) chloride (a_6Ru^{2+}), was prepared by reduction of hexaammineruthenium(III) chloride (Strem Chemicals) with zinc [45]. IR spectra confirmed formation of a_6Ru^{2+} [46] and the product was stored under argon at -20 °C. Immediately before use, a_6Ru^{2+} was dissolved under an argon atmosphere in argon-purged 100 mM NaCl and 10 mM buffer: acetic acid (pH 5), MES (pH 6), NaH_2PO_4 (pH 7), Tris (pH 8), and H_3BO_3 (pH 9). The concentration of a_6Ru^{2+} was determined spectrophotometrically using a Beckman Coulter DU 800 UV/Vis Spectrophotometer with extinction coefficients at 390 nm of 35 $M^{-1}cm^{-1}$ [47] and at 400 nm of 30 $M^{-1}cm^{-1}$ [48]. Absorbance at 550 nm was used to correct for variation in background absorbance. The concentration of a_6Ru^{2+} was evaluated immediately prior to and following stopped-flow mixing. The average and standard deviation of these two measurements is reported as the a_6Ru^{2+} concentration. At the lowest a_6Ru^{2+} concentration, absorbance at 275 nm was also used to evaluate concentration using ε_{275} of 632 $M^{-1}cm^{-1}$, which is the average of the reported extinction coefficients of 624 $M^{-1}cm^{-1}$ [48] and 640 $M^{-1}cm^{-1}$ [47]. Iso-1-Cyt*c* solutions were also prepared in argon-purged buffers. Gas tight syringes were used to transfer iso-1-Cyt*c* and a_6Ru^{2+} solutions to the stopped-flow and UV-Vis instruments. Argon-purged 10 mM buffer in 100 mM NaCl was used to flush the stopped-flow unit prior to use. Heme reduction was followed at 25 °C via 1:1 stopped-flow mixing. Final protein concentration after mixing was 5 μM and a_6Ru^{2+} concentrations were approximately 0.6, 1.25, 2.5, 5, and 10 mM.

Kinetic traces were collected logarithmically with 5000 data points for time periods of 1 to 300 seconds. Data were fit to the appropriate exponential equation using SigmaPlot (version 7.0). For pH 7 and above, a quadruple exponential function was used to fit the data as two slow phases are present under these conditions (Fig. S5). Below pH 7, these slow phases are absent and the data are best fit to a two exponential function (Fig. S5). To accurately capture the slow phases, data were collected on a 150 to 300 second timescale for pH 7, 8 and 9. As the slower phases were absent at pH 5 and 6, long timescale runs were not necessary and data were collected on a 1 to 5 second time scale.

At pH 6-9, one second data sets were also collected using drive pressure holds to reduce recoil noise from the drive syringe, which otherwise can cause artifacts on a timescale similar to the two faster phases. To help constrain the upper baseline of the pH 7 to 9 short timescale data sets, the data were fit to a triple exponential equation and the slow phase rate constant was set equal to $k_{obs,4}$ from the longer timescale fits. $k_{obs,4}$ was used over $k_{obs,3}$ because the associated amplitude was much larger for $k_{obs,4}$ than for $k_{obs,3}$. Typically, 5 and 8 trials were collected for long and short time scale data acquisitions, respectively, for each gated ET experiment.

Results

Global stability of *E. coli*-expressed iso-1-Cyt*c* variants

The global stabilities of the WT* and WT*/K73H iso-1-Cyt*c* variants were determined by GdnHCl denaturation at 25 °C monitored by CD spectroscopy. Denaturation curves of WT* and WT*/K73H variants in Fig. 2 show that the midpoint GdnHCl concentration for unfolding, C_m, is similar for both variants. The unfolding transition of WT*/K73H is also broader than that of WT* (Fig. 2). The K73H mutation causes a decrease of about 1 kcal

mol^{-1} M^{-1} in the *m*-value (rate of change of ΔG_u with respect to GdnHCl concentration), as seen in Table 1. Previously we have demonstrated that GdnHCl unfolding of K73H variants progresses from a partially unfolded His73-heme conformer at pH 7.5, which is responsible for the decreased *m*-value [20, 22, 33]. In the case of WT*/K73H, the free energy of unfolding in the absence of denaturant, $\Delta G_u^{\circ\prime}(H_2O)$, is about 25% lower than that of WT* iso-1-Cyt*c* (Table 1). Comparison with the yeast expressed variants, yWT and yWT/K73H, show that the effect of the tmK72A mutation on global stability is modest [33, 49] (Table 1).

Alkaline conformational transition of WT* and WT*/K73H variants of iso-1-Cyt*c*

Local unfolding of iso-1-Cyt*c* variants at alkaline pH was monitored at 695 nm, an absorbance band which reports on the presence of the native Met80-heme ligand [2, 50, 51]. WT* iso-1-Cyt*c* has a monophasic alkaline conformational transition (Fig. 3). The pK_{app} for WT* was found to be 8.66 ± 0.01, comparable to the value previously reported for yWT of 8.6 ± 0.1 with either a C102T or a C102S mutation [18, 20]. The number of protons, *n*, involved in the conformational change, as determined from a fit of the data to Eq. 1 (Materials and methods), is near 1 (1.15 ± 0.02) for WT* iso-1-Cyt*c*, as expected.

WT*/K73H iso-1-Cyt*c* has a biphasic alkaline conformational transition (Fig. 3). Between pH 6 and 8 a His73-heme ligated conformer populates followed by a Lys79-heme ligated state between pH 8 and 10. Thus, the K73H mutation allows the conformational changes mediated by the residues at positions 73 and 79 to be distinguished readily. WT*/K73H pH titration data were fit using Eq. 2 (Materials and methods). Within error, the pK_a(His) values, which are consistent with the ionization of His73, are similar for both WT*/K73H and yWT/K73H (see Table 2). The conformational equilibrium constant for the alkaline conformational transition mediated by His73, pK_{C1}(His), is more positive for WT*/K73H than for yWT/K73H [20], indicating that the alkaline conformer is less favored when tmK72 is replaced by Ala (Table 2).

Dynamics of the His73-mediated alkaline transition by pH jump methods

In order to elucidate the kinetics of the alkaline transition of the WT*/K73H iso-1-Cyt*c* variant, stopped-flow pH jump methods were employed. Both upward and downward pH jumps were monitored at 406 nm to follow heme-ligand changes produced from Ω-loop D rearrangement. The kinetic data are consistent with three kinetic phases below pH 8 (Tables S2-S6 and Fig. S1). Above approximately pH 8, a fourth kinetic phase becomes evident (Table S3 and Fig. S1). The fast kinetic phase (Fig. S1, observed rate constant, $k_{obs,1}$) occurs on a 100 millisecond timescale. The amplitude of the fast phase increases from pH 6 to pH 8, as expected for the His73-heme alkaline conformer based on thermodynamic data, which shows (see Fig. 3) that equilibrium population of the His73-heme alkaline conformer occurs over this pH range. We also see an increase in amplitude from pH 9 to pH 10 (Table S2).

Near pH 8 and above, an intermediate 1 s time scale phase is observed (Fig. S2, observed rate constant, $k_{obs,2}$). Within error, $k_{obs,2}$ is invariant with pH. Although the amplitude is low, an increase in amplitude between pH 8 and 10 is evident. A similar low amplitude intermediate phase from stopped-flow pH jump experiments that only populates above pH 7.3 has previously been reported for a K79H variant carrying the tmK72A mutation [26].

Stopped-flow conformationally-gated electron transfer (gated ET) experiments on two iso-1-Cyt*c* variants expressed from yeast (i.e., tmK72), AcH73 (this variant has H26N, H33N and H39Q and K73H mutations as well as two mutations near the N-terminus which lead to N-terminal acetylation in vivo [9]) and K73H/K79A [29], exhibit the presence of an intermediate phase from pH 5 to 9 with low amplitude and observed rate constants of a comparable magnitude to values reported here for $k_{obs,2}$. This phase has previously been attributed to a conformational change involving an acid state below pH 7, or a high-spin species above pH 7 [9, 26, 29].

Two slow phases, on a 10 – 100 s timescale are observed. Based on previous work on K73H variants of iso-1-Cyt*c*, these phases likely correspond to formation of a Lys79-heme ligated conformer as well as isomerization of proline in the His73-heme alkaline conformer [29, 30, 42]. The observed rate constant for the first slow phase, $k_{obs,3}$ (Fig. S3), ranges from 0.1 to 0.2 s^{-1}, consistent with the rate of proline isomerization reported for yeast-expressed K73H/K79A iso-1-Cyt*c* (i.e., tmK72) in the same pH regime [29, 42]. The amplitude of this phase shows a modest increase from pH 6 to 8, consistent with the slow phase associated with proline isomerization linked to the His73-heme alkaline transition observed with K73H/K79A iso-1-Cyt*c* [42].

The slowest kinetic phase (Fig. S4) yields an observed rate constant, $k_{obs,4}$, near 0.03 s^{-1} from pH 5 to 8. Above pH 8, $k_{obs,4}$ begins to increase. Corresponding amplitude data for this slow phase also begins to increase near pH 8. The increase in amplitude and observed rate constant for this phase is consistent with thermodynamic data which show that the Lys79-heme ligated conformer populates from pH 8 to 10 (Fig. 3).

Direct measurement of microscopic rate constants for the alkaline transition by gated ET

Gated ET methods were used to directly measure the microscopic rate constants corresponding to Ω-loop D opening and replacement of the native Met80-heme ligand with either histidine or lysine. As previously described [4, 9, 21, 27, 29, 44, 52], oxidized protein with the Met80-heme ligand will undergo direct reduction by hexammineruthenium(II), a_6Ru^{2+} (Fig. 4), whereas the His73-heme alkaline conformer is unable to undergo reduction due to a lower reduction potential [53]. Thus, a conformational change must occur to achieve the native Met80-heme ligated conformer before reduction can occur (Path B in Fig. 4). If the conformational change occurs on a much slower timescale than direct ET, a conformational ET gate exists.

Short time scale data acquisitions at pH 5 and 6 were fit to a two-exponential equation (Fig. S5). These fits are consistent with equilibrium population of both the native Met80-heme ligated conformer and the His73-heme ligated alkaline conformer at these pH values, as illustrated in Fig. 4. Above pH 7, a quadruple exponential equation was needed to fit the data (Fig. S5) indicating the presence of additional conformers with alternate heme ligands at equilibrium in solution that must convert to the native Met80-heme conformer before being reduced by a_6Ru^{2+}. Amplitude and rate constant data for each phase are given in Tables S7-S10. To distinguish them from the observed rate constants from pH jump experiments, we designate the observed rate constants from the gated ET experiments, k_{gET1}, k_{gET2}, k_{gET3}, and k_{gET4}, from fastest to slowest kinetic phase, and the associated

amplitudes as, A_{gET1}, A_{gET2}, A_{gET3} and A_{gET4}. Amplitude data from gated ET experiments are plotted against pH in Fig. 5. When $k_{ET}[a_6Ru^{2+}]$ is much greater than $k_{f,His73}$ (see Fig. 4, or $k_{f,L}$'s, rate constants for formation of conformers with other ligands, L, replacing Met80), individual amplitudes are directly proportional to the population of a given iso-1-Cyt*c* conformer present at each pH because reduction is fast compared to the rate of the conformational change that returns the alternatively ligated conformer to the native state. Values of amplitudes from reduction of WT*/K73H iso-1-Cyt*c* with a_6Ru^{2+} concentrations between 2 and 4 mM were optimal for this purpose. At higher a_6Ru^{2+} concentration, the direct electron transfer rates are fast enough relative to the dead time of our stopped-flow instrument that the associated amplitude may be underestimated (see Fig. S5). Conversely, at lower a_6Ru^{2+} concentrations, $k_{ET}[a_6Ru^{2+}]$ begins to approach $k_{f,His73}$, such that Met80-ligated WT*/K73H can convert to the His73-heme bound conformer before it is reduced, leading to an apparent increase in the amplitude resulting from the His73-heme alkaline conformer (see Table S8).

In Fig. 5, $A_{gET,1}$ shows a decrease in magnitude as pH increases. $A_{gET,1}$ decreases slowly from pH 5 to 7 and then more rapidly above pH 7. This behavior mimics the loss of absorbance at 695 nm due to Fe^{3+}-Met80 ligation as pH is increased in the equilibrium pH titration data in Fig. 3. Thus, the fastest kinetic phase is assigned to WT*/K73H in the native conformer with Met80-heme ligation. $A_{gET,2}$ initially increases as pH is increased above pH 5, maximally populates near pH 7-8, and then decreases. This behavior is consistent with the His73-heme conformer, which should increase in population as pH is increased reaching a maximum when His73 is fully deprotonated near pH 7.5. $A_{gET,3}$ remains relatively invariant from pH 7-9. There is some uncertainty regarding the species corresponding to $A_{gET,3}$, but it may correspond to iso-1-Cyt*c* with a high spin heme as has been observed with other K73H variants of iso-1-Cyt*c* [9, 26, 29]. The equilibrium population of this species is clearly small (Fig. 5), so, absorbance features near 650 nm, typical of a high spin heme, are not evident in equilibrium pH titration data (not shown). $A_{gET,4}$, grows from a minor phase at pH 7 to the largest amplitude at pH 9. The increase in $A_{gET,4}$ as $A_{gET,1}$ and $A_{gET,2}$ decrease is consistent with the behavior expected for the Lys79-heme conformer. Lys79 is expected to displace both Met80 and His73 as the heme ligand at high pH. The pH dependence of amplitude data from gated ET experiments observed here is similar to that previously reported for AcH73 iso-1-Cyt*c* [9].

The magnitude of the rate constant for the fastest phase of the gated ET experiment, $k_{gET,1}$, is strongly dependent on the concentration of a_6Ru^{2+} consistent with direct ET with bimolecular rate constant, k_{ET} (Fig. 4), to the native state of WT*/K73H iso-1-Cyt*c* (Table S7 and Fig. S6). The other rate constants from the gated ET experiments show little dependence on the concentration of a_6Ru^{2+} (Fig. S7 and Tables S8 to S10). Thus, these rate constants reflect reduction of WT*/K73H iso-1-Cyt*c* gated by a conformational change.

Discussion

Effects of the tmK72A mutation on the global and local stability of yeast iso-1-Cyt*c*

The crystal structure of yeast iso-1-Cyt*c* shows that tmK72 lies across Ω-loop D, potentially sterically hindering opening of the heme crevice (Fig. 1 and Fig. 8, below). Previously, we

have shown that for variants of iso-1-Cyt*c* carrying a K79H mutation, similar stability parameters are obtained from GdnHCl denaturation regardless of whether trimethyllysine or alanine is present at residue 72 [26]. Here, within error, we also report only a modest effect of the tmK72A mutation on the stability of a K73H variant of iso-1-Cyt*c* (Table 1). Similarly, the tmK72A mutation does not affect the global stability of iso-1-Cyt*c* (yWT versus WT* in Table 1)

Global unfolding experiments were performed at pH 7.5 where WT*/K73H partially populates the His73-heme conformer as is apparent from Figs. 3 and 5. The decrease in the denaturant *m*-value of WT*/K73H iso-1-Cyt*c* relative to WT* iso-1-Cyt*c* (see Table 1) is consistent with global unfolding monitored by CD occurring primarily from the partially unfolded His73-heme alkaline conformer as for other K73H variants of iso-1-Cyt*c* [21, 33, 42].

pH titration studies demonstrate that pK_{app} is similar for WT* iso-1-Cyt*c* and yWT iso-1-Cyt*c* indicating that the tmK72A mutation has little effect on the Lys-mediated alkaline conformational transition. When the K73H mutation is introduced, within error pK_{C2}(Lys), which corresponds to the Lys79-mediated alkaline transition, is also unaffected by the tmK72A mutation (Table 2). However, pK_{C1}(His), which corresponds to the His73-mediated alkaline transition is about twice the positive magnitude for WT*/K73H compared to yWT/K73H (Table 2). Thus, the tmK72A mutation destabilizes the His73-heme alkaline conformer relative to the native conformer (ΔΔG of 0.53 ± 0.09 kcal/mol). By contrast, data in Table 2 for previously reported K79H variants of iso-1-Cyt*c*, show that tmK72A mutation has little effect on the stability of the His79-heme alkaline conformer relative to the native conformer [26]. Interestingly, the tmK72A mutation makes pK_{C2}(Lys) for the Lys73-heme alkaline conformer less favorable relative to the native conformer (ΔΔG of 0.45 ± 0.31 kcal/mol) for K79H variants. Thus, the tmK72A mutation appears to have less effect on the stability of alkaline conformers relative to the native state when the alkaline state ligand is from position 79, whereas it appears to destabilize the alkaline conformer relative to the native conformer by about 0.5 kcal/mol when the ligand is from position 73. Thus, the Ω-loop D substructure (Red in Fig. 1) clearly responds differently to the tmK72A mutation when deformed from position 73 versus position 79.

Histone binding proteins interact with trimethyllysine residues on histone tails using aromatic cage motifs, which are rich in aromatic residues (Tyr, Phe, Trp) and methionine [54, 55]. Trimethyllysine binding is stabilized by π-cation interactions. In the NMR structure of the Lys73-heme alkaline conformer [10], Met80 and Tyr67 are proximal to the side chain of position 72 providing a potential aromatic cage-like motif to bind tmK72 that could stabilize alkaline conformers with His/Lys73-heme ligation (see Fig. 8 below).

The tmK72A mutation affects the dynamics of the His73-mediated alkaline transition at both low and high pH

Fig. 6 compares the pH dependence of $k_{obs,1}$ from pH jump experiments for the His73-heme alkaline conformational transition of WT*/K73H to previously reported data for yWT/K73H [30]. Below pH 6, $k_{obs,1}$ remains constant for WT*/K73H whereas it increases for yWT/K73H [30]. Between pH 6 and 8, $k_{obs,1}$ is identical for the two variants. From pH 8 to 10,

$k_{obs,1}$ initially increases more slowly with increasing pH for WT*/K73H compared to yWT/K73H. Thus, except for near neutral pH the tmK72A mutation significantly affects $k_{obs,1}$. This behavior contrasts sharply with the effect of the tmK72A mutation on the dynamics of the His79-heme alkaline transition. In this case, the change in dynamics caused by the mutation is more pronounced near neutral pH and less pronounced near pH 5 and 10 [26, 27]. The mechanism of the alkaline transition is different when mediated by His73 than when mediated by His79. In general, three ionizable groups are required to fit kinetic data for the His73-mediated alkaline transition [9, 29, 30, 42], while only two are required to fit the kinetics of the His79-mediated alkaline transition [23, 26, 27]. Thus, it is perhaps not surprising that the two alkaline transitions respond differently to the tmK72A mutation.

Normally the His73-mediated alkaline conformational transition is best fit to a model involving three ionizable groups. Since the ionizable group with a pK_a near 5.5 (pK_{H1} in ref. [30]) is not evident for WT*/K73H (Fig. 6) we fit the $k_{obs,1}$ versus pH data to a model involving two ionizable groups (Fig. 6b) [23, 30].

This model yields Eq. 3 for the pH dependence of $k_{obs,1}$.

$$k_{obs,1} = \left(\frac{K_{HL}}{K_{HL} + [\mathrm{H}^+]}\right) * \left(\frac{k_{f1,His} * [\mathrm{H}^+] + k_{f2,His} * K_{H2}}{K_{\mathrm{H2}} + [\mathrm{H}^+]}\right) + \left(\frac{k_{b1,His} * [\mathrm{H}^+] + k_{b2,His} * K_{\mathrm{H2}}}{K_{\mathrm{H2}} + [\mathrm{H}^+]}\right) \quad (3)$$

In Eq. 3, the methionine-heme to histidine-heme ligand conformational switch corresponds to forward rate constant, $k_{f1,His}$, near neutral pH and the reverse rate constant for the conformational switch is $k_{b1,His}$. K_{HL} (or pK_{HL}) is the ionization constant for the ligand (His73 in this case) which replaces Met80. As a result of the second ionization event (K_{H2} or pK_{H2}), the rate constants change to $k_{f2,His}$ and $k_{b2,His}$. In this model, $k_{b1,His}$ is equal to $k_{obs,1}$ at low pH where the native conformer is fully populated. $k_{b2,His}$ cannot be determined directly from the $k_{obs,1}$ versus pH data. From amplitude data, we can estimate the K_{C1}(His) at pH values above pK_{H2}, $K_{C1}(His)_{Hi}$, to be 0.94 (see Electronic supplementary material). With this value for $K_{C1}(His)_{Hi}$ as a constraint, $k_{f2,His}$ and $k_{b2,His}$ can be obtained from the fit of Eq. 3 to the $k_{obs,1}$ versus pH data for WT*/K73H iso-1-Cyt*c* in Fig. 6a. The parameters from the fit of the $k_{obs,1}$ versus pH data for WT*/K73H in Fig. 6a are summarized in Table 3. Compared to yWT/K73H the forward rate constant, $k_{f1,His}$, is similar but, $k_{b1,His}$ is larger for WT*/K73H, consistent with the destabilizing effect of the tmK72A mutation on the His73-heme alkaline conformer observed in our thermodynamic data (Table 2).

The behavior of the K73H variants is quite opposite of that of the K79H variants. $k_{b1,His}$ is unaffected by the tmK72A mutation with the K79H variants whereas $k_{f1,His}$ increases by 1.5- to 2.5-fold [26, 27]. It is also noteworthy that following the second ionization event for K79H variants, the magnitude of $k_{obs,1}$ decreases [23, 26, 27], opposite of what occurs with K73H variants [9, 29, 30, 42].

The pK_{HL} from fitting the $k_{obs,1}$ versus pH data for WT*/K73H iso-1-Cyt*c* in Fig. 6a has a higher value than the pK_a(His) of about 6.7, reported in Table 2 from pH titration data. The amplitude versus pH data for the His73-heme alkaline transition shows two phases (Fig. 7).

Thus, we can also fit the amplitude versus pH data to obtain values for pK_{HL} and pK_{H2} using Eq. 4 [23, 30], which describes the behavior of the amplitude of the His73-heme alkaline transition

$$\text{Amplitude}=C_{\text{T}} * \left\{ \frac{\left(\frac{K_{HL}}{K_{HL}+[H^+]}\right)}{\left(\frac{K_{HL}}{K_{HL}+[\text{H}^+]}\right)+\left(\frac{k_{\text{b1},His}*[\text{H}^+]+k_{\text{b2},His}*K_{\text{H2}}}{K_{\text{f1},His}*[\text{H}^+]+k_{\text{f2},His}*K_{\text{H2}}}\right)} \right\} \quad (4)$$

expected for the two ionization mechanism (Fig. 6b). In Eq. 4, C_{T} is the amplitude if the conformational transition goes to completion. In fitting the data, the microscopic rate constants ($k_{\text{f1,His}}$, $k_{\text{b1,His}}$, $k_{\text{f2,His}}$ and $k_{\text{b2,His}}$) from the fit of the $k_{\text{obs,1}}$ versus pH data in Fig. 6a (Table 3) were used as constants in Eq. 4. The fit of the data yields a value for pK_{HL} of 6.8 ± 0.1 which is in good agreement with the pK_a(His) obtained from thermodynamic data (Table 2). This value for pK_{HL} is likely more reliable than the one obtained from the $k_{\text{obs,1}}$ versus pH data, given the size of errors bars and the scatter in the $k_{\text{obs,1}}$ data below pH 7. Within error the value for pK_{H2} did not change whether fitting $k_{\text{obs,1}}$ or amplitude versus pH data (Table 3). It is possible that a third ionization event may occur at a lower pH, however, within the error of the reported data points we are unable to reliably detect this ionization, which is clearly present for yWT/K73H iso-1-Cyt*c* (Fig. 6). pK_{HL} is similar for both WT*/K73H and yWT/K73H [30]. However, pK_{H2} increases by about 1 unit for WT*/K73H compared to yWT/K73H (Table 3). By contrast, the tmK72A mutation does not affect pK_{H2} for the His79-heme alkaline transition. We previously speculated that the outer heme propionate (also referred to as heme propionate-7 and heme propionate D), which is believed to have a pK_a greater than 9 [2, 56, 57], could be responsible for the pK_{H2} ionization [23]. If our earlier speculation is correct, the tmK72A mutation increases the pK_a of the outer heme propionate in the context of the K73H mutation, but not in the context of the K79H mutation [26]. In summary, our kinetic data also show that the effect of the tmK72A mutation depends on whether Ω-loop D is deformed from position 73 or 79.

Determining forward and reverse rate constants of the alkaline conformational transition

The individual rate constants from the gated ET experiments were plotted against a_6Ru^{2+} concentration. $k_{\text{gET,1}}$, which corresponds to bimolecular ET from a_6Ru^{2+} to the native state, shows a linear dependence on a_6Ru^{2+} concentration (Fig. S6) as expected for a bimolecular reaction under pseudo-first-order conditions (see Fig. 4). Fitting the $k_{\text{gET,1}}$ versus a_6Ru^{2+} concentration data to Eq. 5, yields the bimolecular rate constant k_{ET} as the slope. In Eq. 5, k_{uni}

$$k_{gET,1}=k_{ET} * \left[a_6Ru^{2+}\right]+k_{uni} \quad (5)$$

represents a summation of all unimolecular rate constants ($k_{\text{f,His}}$, see Fig. 4, and $k_{\text{f,L}}$'s for species corresponding to $A_{\text{gET,3}}$ and $A_{\text{gET,4}}$, see Fig. 5) that lead to the disappearance of the native conformer. The k_{ET} values as a function of pH are listed in Table 4 and plotted in Fig. S6. k_{ET} values decrease with increasing pH. A similar pH dependence for k_{ET} is observed for the AcH73 variant of iso-1-Cyt*c* [9], as well as, for a yWT/K73H/K79A variant of iso-1-Cyt*c* [29] both of which contain the native tmK72 residue. This observation suggests that the

mechanism of direct ET is similar, regardless of whether Ω-loop D is sterically hindered by tmK72 or sterics have been relieved by the tmK72A mutation.

By contrast, k_{ET} for reduction of WT*/K79H increases as pH increases [27]. The relative proximity of His73 versus His79 to the heme may account for these differences. At higher pH, deprotonation of His79, which is close to the heme edge (see Fig. 1), will make it easier for a_6Ru^{2+} to form a precursor complex [58], which has a_6Ru^{2+} close to the heme of iso-1-Cyt*c*. Thus, the observed increase in k_{ET} as pH increases is reasonable. His73 is located above Met80 far removed from the heme edge (see Fig. 1). Deprotonation of His 73 would thus increase the probability that a_6Ru^{2+} would form a precursor complex with Cyt*c* at a greater distance from the heme edge. At this location, ET is expected be less favorable, leading to the observed drop in k_{ET} at higher pH.

At all pH values, the magnitude of $k_{gET,2}$, which corresponds to reduction of the His73-heme conformer, is independent of a_6Ru^{2+} concentration at high concentrations of a_6Ru^{2+}. Evidently at high a_6Ru^{2+} concentration, $k_{ET}[a_6Ru^{2+}]$ is much greater than $k_{f,His}$, such that the rate of reduction is controlled by the unimolecular conformational change back to the native state (i.e., $k_{gET,2}$ is approximately equal to $k_{b,His}$, see Eq 6 and Fig. 4). At pH 8 and 9, there is some decrease in $k_{gET,2}$ at the lowest concentrations of a_6Ru^{2+}. Thus, it is possible to fit the dependence of $k_{gET,2}$ on a_6Ru^{2+} concentration to the full form of Eq. 6, which is derived assuming a steady-state approximation [59-61], so that both rate constants, $k_{b,His}$ and $k_{f,His}$, associated with the

$$k_{gET,2}=\frac{\left(k_{b,His}k_{ET}\left[a_6Ru^{2+}\right]\right)}{\left(k_{f,His}+k_{ET}\left[a_6Ru^{2+}\right]\right)} \quad (6)$$

conformational transition can be obtained (Fig. S7). At pH 7 and below, no clear decrease in $k_{gET,2}$ is observed at the lowest a_6Ru^{2+} concentrations. The data at pH 7 were fit to Eq. 6, to obtain $k_{b,His}$. The fit also provides $k_{f,His}$, but the error in its magnitude is large (Table 4) and at best it provides an upper limit for $k_{f,His}$ at pH 7. At pH 5 and 6, the errors in the magnitudes of $k_{gET,2}$ are larger, so, we have used the average of $k_{gET,2}$ at all concentrations of a_6Ru^{2+} as an estimate for the magnitude of $k_{b,His}$. All values of $k_{f,His}$ and $k_{b,His}$ obtained from gated ET experiments are reported in Table 4.

In Fig. 6a, the microscopic rate constants, $k_{f,His}$ and $k_{b,His}$, obtained from the gated ET experiments along with their sum, which should be equal to $k_{obs,1}$ obtained from pH jump experiments, are plotted against $k_{obs,1}$ for the His73-heme alkaline transition obtained from pH jump experiments. Across the pH regime studied, values for $k_{b,His}$ are invariant within error for WT*/K73H, except at pH 9 where $k_{b,His}$ appears to increase by about 10% (Table 4). For yWT/K73H and other variants with K73H mutations, an ionizable group with a pK_a near 5.5 is observed (see Fig. 6 and refs. [9, 29]). If there is an ionization affecting the His73-heme alkaline transition in this pH regime, its effect on the magnitude of $k_{b,His}$ is within the error of our measurements. As the pH is increased, the rate constant associated with opening of the heme crevice and replacing the methionine-heme ligand with histidine, $k_{f,His}$, increases. Below pH 7, $k_{f,His}$ is too small to evaluate. At pH 5 and 6, $k_{b,His}$ is within

error of the magnitude of $k_{obs,1}$ from pH jump experiments (Fig. 6a), indicating that $k_{f,His}$ is close to zero. At pH 7 and above, the sum of $k_{f,His}$ and $k_{b,His}$ matches $k_{obs,1}$ from pH jump experiments reasonably well (Fig. 6a). At pH 8, where the His73-heme alkaline conformer is maximally populated (Fig. 5), the ratio of $k_{f,His}$ to $k_{b,His}$ should be close to K_{C1}(His) obtained from equilibrium measurements. At pH 8, K_{C1}(His) (obtained as $k_{f,His}$ divided by $k_{b,His}$) equals 0.32 ± 0.08, which is close to K_{C1}(His) of 0.21 ± 0.02 from equilibrium data for WT*/K73H (derived from pK_{C1}(His) in Table 2). At pH 9, $k_{f,His}$ and $k_{b,His}$ yield 0.7 ± 0.1 for K_{C1}(His). This value approaches our estimate of the increase from K_{C1}(His) near 0.21 to $K_{C1}(His)_{Hi}$ of about 0.94 due to the ionization of the group with pK_{H2} of 10 (Fig. 7 and Table 3). Interestingly, the pK_{H2} ionization also increases the stability of the His73-heme conformer relative to the native conformer for the AcH73 variant of iso-1-Cyt*c* [29].

Effect of the tmK72A mutation on the free energy landscape of K73H variants of iso-1-Cyt*c*

Fig. 8 shows the effect of the tmK72A mutation on the free energy landscape of the His73-mediated alkaline transition of iso-1-Cyt*c* using thermodynamic and kinetic data presented here for WT*/K73H and reported previously for yWT/K73H [20, 30]. In Fig. 8, we have assumed that the tmK72A mutation does not affect the stability of the native state. This choice is partially dictated by the small decrease in the stability of the His73-heme conformer based on GdnHCl unfolding data in Table 1 (given that global unfolding of K73H variants proceeds primarily from the His73-heme conformer, ref. [20]), which is similar in magnitude to the effect of the tmK72A mutation on the relative stability of the native conformer versus the His73-heme alkaline conformer (Table 2). As discussed above, the NMR structure of the Lys73-heme alkaline conformer suggests that tmK72 could interact with an aromatic cage-like motif [54, 55], derived from Tyr67 and Met80 in the Lys/His73-heme alkaline conformer [10, 26]. Truncation of tmK72 to an Ala would eliminate this interaction [10] (see Fig. 8, lower right), supporting the contention that the increase in the positive magnitude of pK_{C1}(His) (less favorable equilibrium) results primarily from a destabilization of the His73-heme conformer with little effect on the free energy of the native state (Fig. 8). The lesser effect of the tmK72A mutation on the transition state (TS, see Fig. 8) would be consistent with partial formation of the aromatic cage-like motif in the TS. Assigning effects of mutations to one ground state or another is always uncertain. The global stability of the yWT/K73H is sensitive to how the global unfolding data are fit and could be somewhat lower than for the WT*/K73H variant [62]. Also, the overlap between partial unfolding to the His73-heme alkaline conformer by GdnHCl and global unfolding is likely greater for the WT*/K73H variant than for the yWT/K73H variant because the His73-heme alkaline conformer is destabilized by the tmK72A mutation (Table 2). Thus, the estimation of the free energy of the His73-heme alkaline conformer for WT*/K73H iso-1-Cyt*c* versus yWT/K73H iso-1-Cyt*c* has some uncertainty. The discussion here is supported by structural data for the Lys73-heme alkaline conformer (Fig. 8, lower right) [10]. However, the factors affecting the stabilities of the two ground states as a result of the tmK72A mutation may be more complex. What is clear is that tmK72A mutation decreases the barrier from the His73-heme alkaline conformer to the TS and may cause a slight increase in the barrier from the native conformer to the TS (although the errors in $k_{f,His}$ for WT*/K73H and yWT/K73H are overlapping, see Fig. 8).

Thus, the tmK72A mutation has very different effects on the free energy landscape of Ω-loop D with respect to formation of a His73-heme versus a His79-heme alkaline conformer. For the His79-heme alkaline transition, the tmK72A mutation decreases the barrier from the native conformer to the TS allowing faster formation of the His79-heme alkaline conformer [26, 27]. For the His73-heme alkaline transition, the tmK72A mutation decreases the barrier from the His73-heme alkaline conformer to the TS speeding formation of the native conformer. This observation has interesting general implications for the effects of mutations on the tier 0 dynamics of protein substructures involved in function. In particular, our results show that the dynamic accessibility of different higher energy states of a protein substructure can be affected differently by mutation, which could change the partitioning between different functions or modulate the specificity of a function. In the case of iso-1-Cyt*c*, peroxidase activity is enhanced by the tmK72A mutation [25], suggesting that the tier 0 dynamics required to access the higher energy state of Ω-loop D that mediates peroxidase activity may be similar to the tier 0 dynamics required to access the His79-heme alkaline conformer but not those to access His73-heme alkaline conformer. Given the high conservation of Ω-loop D between yeast and mammals, it is possible that the residue at position 72 has similar effects on the tier 0 dynamics required for peroxidase activity early in apoptosis for mammalian Cyt*c*.

Conclusion

The primary observation of the present work is that the effect of the tmK72A mutation on the His73-heme alkaline transition is entirely opposite from that observed for the His79-heme alkaline transition. Near neutral pH, this mutation destabilizes the His73-heme alkaline conformer relative to the native conformer, whereas it destabilizes the native conformer relative to the His79-heme alkaline conformer. This mutation also enhances the rate of formation of the His79-heme alkaline conformer near neutral pH while enhancing the rate of formation of the native conformer from the His73-heme alkaline conformer. Therefore, the effect of the tmK72A mutation on the dynamics of Ω-loop D clearly depends of the nature of the deformation of this substructure. Peroxidase activity assays on yWT versus WT* iso-1-Cyt*c* show that k_{cat} is 2-fold larger near pH 8 for WT* iso-1-Cyt*c*, which carries the tmK72A mutation [25]. Given the high degree of conservation of Ω-loop D from yeast to mammals, and the current results on the effect of the tmK72A mutation on the dynamics of the His73-heme alkaline transition, our previous peroxidase activity results suggest that the dynamics of heme crevice opening required for peroxidase activity early in apoptosis may be similar to the dynamics of Ω-loop D which lead to formation of the His79-heme alkaline conformer.

Supplementary Material

Refer to Web version on PubMed Central for supplementary material.

Acknowledgments

This research was supported by NSF grants CHE-0910166 and CHE-1306903 to B.E.B. The Bruker microflex MALDI-ToF mass spectrometer was acquired with support from an NSF Major Research Instrumentation Grant CHE-1039814. B.E.B. also acknowledges support from CoBRE grant P20GM103546 funded by the NIGMS.

Abbreviations

ET	electron transfer
gated ET	Conformationally-gated electron transfer
GdnHCl	guanidine hydrochloride
iso-1-Cyt*c*	iso-1-cytochrome *c*
tmK	trimethyllysine

References

1. Henzler-Wildman K, Kern D. Nature. 2007; 450:964–972. [PubMed: 18075575]
2. Moore, GR.; Pettigrew, GW. Cytochromes c: Evolutionary, Structural and Physicochemical Aspects. Springer-Verlag; New York: 1990.
3. Kagan VE, Bayir HA, Belikova NA, Kapralov O, Tyurina YY, Tyurin VA, Jiang J, Stoyanovsky DA, Wipf P, Kochanek PM, Greenberger JS, Pitt B, Shvedova AA, Borisenko G. Free Radical Biol. Med. 2009; 46:1439–1453. [PubMed: 19285551]
4. Cherney MM, Bowler BE. Coord. Chem. Rev. 2011; 255:664–677.
5. Ansari A, Berendzen J, Bowne SF, Frauenfelder H, Iben IET, Sauke TB, Shyamsunder E, Young RD. Proc. Natl. Acad. Sci. U.S.A. 1985; 82:5000–5004. [PubMed: 3860839]
6. Banci L, Bertini I, Rosato A, Varani G. J. Biol. Inorg. Chem. 1999; 4:824–837. [PubMed: 10631615]
7. Berghuis AM, Brayer GD. J. Mol. Biol. 1992; 223:959–976. [PubMed: 1311391]
8. Barker PD, Mauk AG. J. Am. Chem. Soc. 1992; 114:3619–3624.
9. Bandi S, Bowler BE. Biochemistry. 2011; 50:10027–10040. [PubMed: 22026475]
10. Assfalg M, Bertini I, Dolfi A, Turano P, Mauk AG, Rosell FI, Gray HB. J. Am. Chem. Soc. 2003; 125:2913–2922. [PubMed: 12617658]
11. Döpner S, Hildebrandt P, Rosell FI, Mauk AG, von Walter M, Buse G, Soulimane T. Eur. J. Biochem. 1999; 261:379–391. [PubMed: 10215847]
12. Döpner S, Hildebrandt P, Rosell FI, Mauk AG. J. Am. Chem. Soc. 1998; 120:11246–11255.
13. Krishna MM, Maity H, Rumbley JN, Lin Y, Englander SW. J. Mol. Biol. 2006; 359:1410–1419. [PubMed: 16690080]
14. Krishna MM, Lin Y, Rumbley JN, Englander SW. J. Mol. Biol. 2003; 331:29–36. [PubMed: 12875833]
15. Bai Y, Sosnick TR, Mayne L, Englander SW. Science. 1995; 269:192–197. [PubMed: 7618079]
16. Laun, P.; Buettner, S.; Rinnerthaler, M.; Burhans, WC.; Breitenbach, M. Subcellular Biochemistry: Aging Research in Yeast. Breitenbach, M.; Jazwinski, SM.; Laun, P., editors. Springer; Netherlands: 2012. p. 207-232.
17. Ferrer JC, Guillemette JG, Bogumil R, Inglis SC, Smith M, Mauk AG. J. Am. Chem. Soc. 1993; 115:7507–7508.
18. Rosell FI, Ferrer JC, Mauk AG. J. Am. Chem. Soc. 1998; 120:11234–11245.
19. Blouin C, Guillemette JG, Wallace CJA. Biophys. J. 2001; 81:2331–2338. [PubMed: 11566802]
20. Nelson CJ, Bowler BE. Biochemistry. 2000; 39:13584–13594. [PubMed: 11063596]
21. Bandi S, Bowler BE. J. Am. Chem. Soc. 2008; 130:7540–7541. [PubMed: 18494471]
22. Kristinsson R, Bowler BE. Biochemistry. 2005; 44:2349–2359. [PubMed: 15709747]
23. Bandi S, Baddam S, Bowler BE. Biochemistry. 2007; 46:10643–10654. [PubMed: 17713929]
24. Pollock WB, Rosell FI, Twitchett MB, Dumont ME, Mauk AG. Biochemistry. 1998; 37:6124–6131. [PubMed: 9558351]
25. McClelland LJ, Mou T-C, Jeakins-Cooley ME, Sprang SR, Bowler BE. Proc. Natl. Acad. Sci. U.S.A. 2014; 111:6648–6653. [PubMed: 24760830]

26. Cherney MM, Junior C, Bowler BE. Biochemistry. 2013; 52:837–846. [PubMed: 23311346]
27. Cherney MM, Junior CC, Bergquist BB, Bowler BE. J. Am. Chem. Soc. 2013; 135:12772–12782. [PubMed: 23899348]
28. Kostrzewa A, Páli T, Wojciech F, Marsh D. Biochemistry. 2000; 39:6066–6074. [PubMed: 10821679]
29. Bandi S, Bowler BE. Biopolymers (Pept Sci). 2013; 100:114–124.
30. Martinez RE, Bowler BE. J. Am. Chem. Soc. 2004; 126:6751–6758. [PubMed: 15161303]
31. Myers JK, Pace CN, Scholtz JM. Protein Sci. 1995; 4:2138–2148. [PubMed: 8535251]
32. Schellman JA. Biopolymers. 1978; 17:1305–1322.
33. Godbole S, Dong A, Garbin K, Bowler BE. Biochemistry. 1997; 36:119–126. [PubMed: 8993325]
34. Duncan MG, Williams MD, Bowler BE. Protein Sci. 2009; 18:1155–1164. [PubMed: 19472325]
35. Rosell FI, Mauk AG. Biochemistry. 2002; 41:7811–7818. [PubMed: 12056913]
36. Rumbley JN, Hoang L, Englander SW. Biochemistry. 2002; 41:13894–13901. [PubMed: 12437346]
37. Deng WP, Nickoloff JA. Anal. Biochem. 1992; 200:81–88. [PubMed: 1595905]
38. Redzic JS, Bowler BE. Biochemistry. 2005; 44:2900–2908. [PubMed: 15723532]
39. Wandschneider E, Hammack BN, Bowler BE. Biochemistry. 2003; 42:10659–10666. [PubMed: 12962490]
40. Pace CN. Methods Enzymol. 1986; 131:266–280. [PubMed: 3773761]
41. Hammack BN, Smith CR, Bowler BE. J. Mol. Biol. 2001; 311:1091–1104. [PubMed: 11531342]
42. Baddam S, Bowler BE. Biochemistry. 2005; 44:14956–14968. [PubMed: 16274242]
43. Margoliash E, Frohwirt N. Biochem. J. 1959; 71:570–572. [PubMed: 13638266]
44. Baddam S, Bowler BE. J. Am. Chem. Soc. 2005; 127:9702–9703. [PubMed: 15998071]
45. Fergusson JE, Love JL. Inorganic Synthesis. 1972; 13:208–213.
46. Allen AD, Senoff CV. Can. J. Chem. 1967; 45:1337–1341.
47. Matsubara T, Ford PC. Inorg. Chem. 1978; 17:1747–1752.
48. Meyer TJ, Taube H. Inorg. Chem. 1968; 7:2369–2370.
49. Godbole S, Hammack B, Bowler BE. J. Mol. Biol. 2000; 296:217–228. [PubMed: 10656828]
50. Eaton WA, Hochstrasser RM. J. Chem. Phys. 1967; 46:2533–2539. [PubMed: 6039380]
51. Dragomir I, Hagarman A, Wallace C, Schweitzer-Stenner R. Biophys. J. 2007; 92:989–998. [PubMed: 17098790]
52. Baddam S, Bowler BE. Inorg. Chem. 2006; 45:6338–6346. [PubMed: 16878944]
53. Bortolotti CA, Paltrinieri L, Monari S, Ranieri A, Borsari M, Battistuzzi G, Sola M. Chem Sci. 2012; 3:807–810.
54. Sanchez R, Zhou M-M. Trends Biochem. Sci. 2011; 36:364–372. [PubMed: 21514168]
55. Daze KD, Hof F. Acc. Chem. Res. 2013; 46:937–945. [PubMed: 22724379]
56. Hartshorn RT, Moore GR. Biochem. J. 1989; 258:595–598. [PubMed: 2539812]
57. Moore GR. FEBS Lett. 1983; 161:171–175. [PubMed: 6311622]
58. Cusanovich, MA.; Tollin, G. Cytochrome c: A Multidisciplinary Approach. Scott, RA.; Mauk, AG., editors. University Science Books; Sausalito, CA: 1996. p. 489-513.
59. Wijetunge P, Kulatilleke CP, Dressel LT, Heeg MJ, Ochrymowycz LA, Rorabacher DB. Inorg. Chem. 2000; 39:2897–2905. [PubMed: 11232830]
60. Meagher NE, Juntunen KL, Salhi CA, Ochrymowycz LA, Rorabacher DB. J. Am. Chem. Soc. 1992; 114:10411–10420.
61. Rorabacher DB. Chem. Rev. 2004; 104:651–697. [PubMed: 14871138]
62. Godbole S, Bowler BE. Biochemistry. 1999; 38:487–495. [PubMed: 9890932]

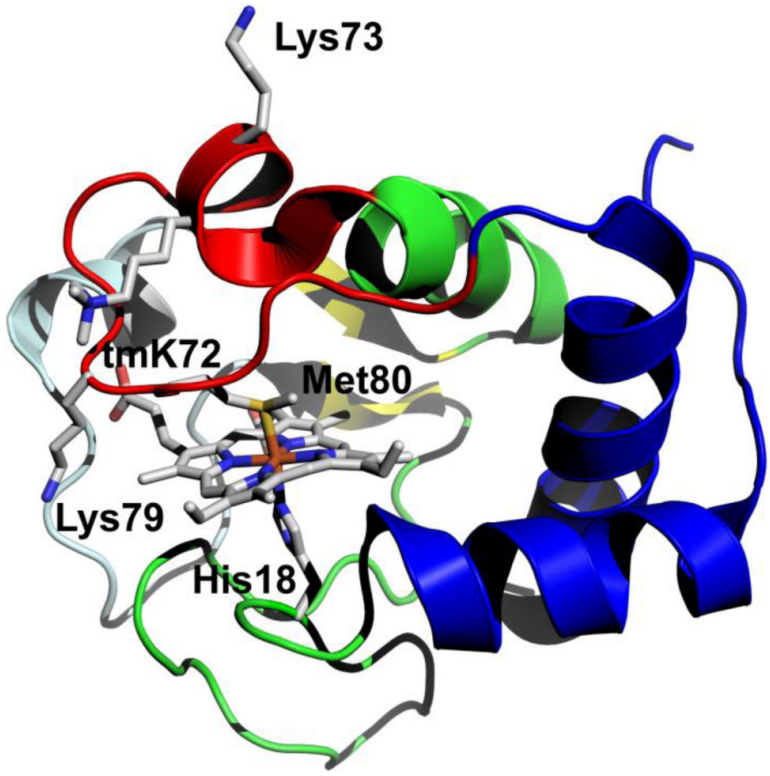

Fig. 1.

Structure of iso-1-Cyt*c* (pdb code: 2YCC, [7]). The loop shown in red is Ω-loop D and provides Met80 as a heme ligand in the native state. Lysines 73 and 79 provide the alkaline state ligands for wild type iso-1-Cyt*c*. Lysine 72 is trimethylated, tmK72, when iso-1-Cyt*c* is expressed in its native host yeast. tmK72 can be seen to lie across the surface of the heme crevice loop, Ω-loop D. The cooperative substructures of Cyt*c*, as defined by Englander and coworkers [13-15], from least to most stable are color-coded: pale cyan, red, yellow, green and blue

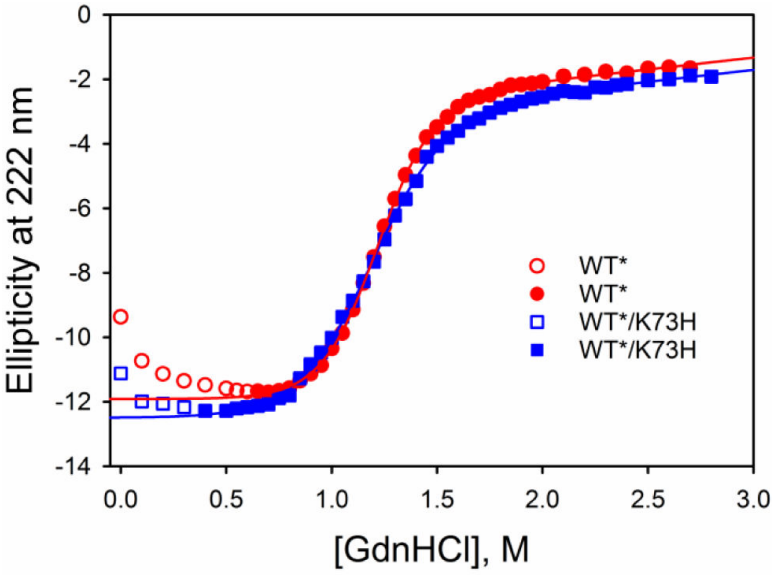

Fig. 2.

GdnHCl denaturation curves for the WT* (red circles) and WT*/K73H (blue squares) variants of iso-1-Cyt*c*. Unfolding was monitored at 222 nm as GdnHCl was titrated into iso-1-Cyt*c* buffered with 40 mM NaCl, 20 mM Tris buffer, pH 7.5 at 25 °C. Data in open symbols were not included in the fit to a two-state model (solid curves), described in the Materials and methods.

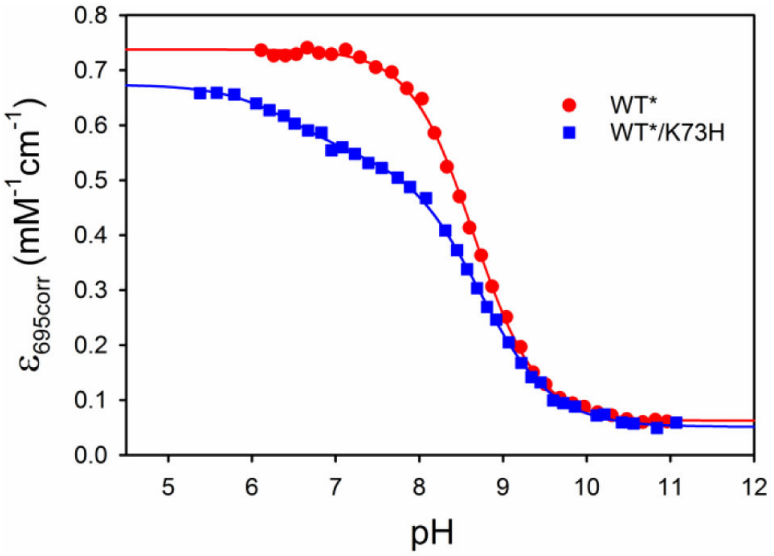

Fig. 3.

$\varepsilon_{695corr}$ vs pH data for the WT* (red circles) and WT*/K73H (blue squares) variants of iso-1-Cyt*c*, which monitor the alkaline conformational transition of iso-1-Cyt*c*. WT* iso-1-Cyt*c* displays a monophasic transition (solid red curve is a fit to Eq. 1 in Materials and methods) and WT*/K73H shows a biphasic transition (solid blue curve is a fit to Eq. 2 in Materials and methods). Data were acquired in 100 mM NaCl at 22 ± 1 °C.

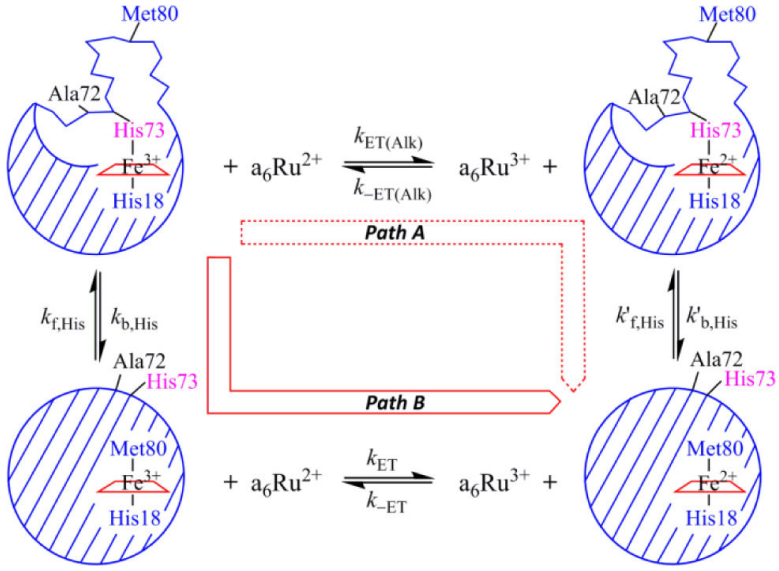

Fig. 4.

Gated ET square scheme for the WT*/K73H variant showing paths A and B.

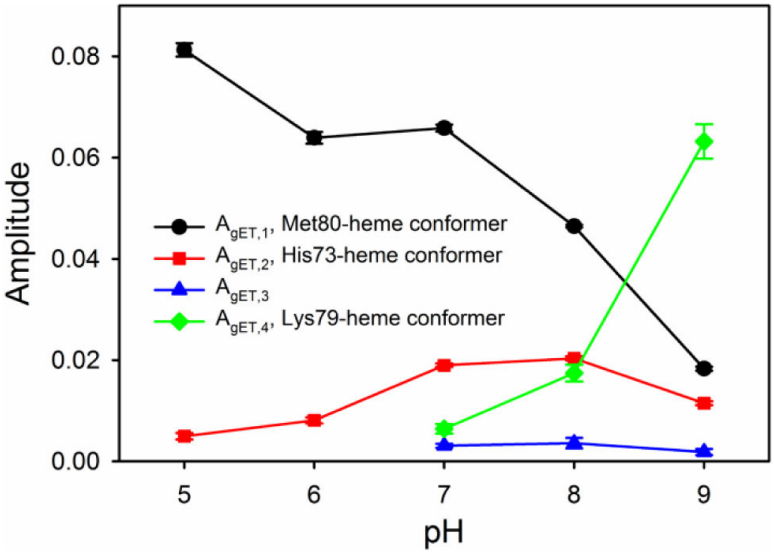

Fig. 5.

Amplitude data vs pH from gated ET experiments on WT*/K73H. Amplitude values correspond to the change in absorbance at 550 nm. Concentrations of a_6Ru^{2+} for $A_{gET,1}$ (black circles and line) and $A_{gET,2}$ (red squares and line) for pH 5, 6, 7, 8 and 9 were 2.8, 3.0, 3.7, 3.9 and 2.8 mM, respectively. $A_{gET,1}$ and $A_{gET,2}$ are both from short (1 to 5 s) data acquisitions, Concentrations of a_6Ru^{2+} for $A_{gET,3}$ (blue triangles and line) and $A_{gET,4}$ (green diamonds and line) for pH 7, 8 and 9 were 1.9, 2.24 and 1.78 mM, respectively. $A_{gET,3}$ and $A_{gET,4}$ are both from long timescale (150 to 300 s) data acquisitions. Error bars are the standard deviation of the average.

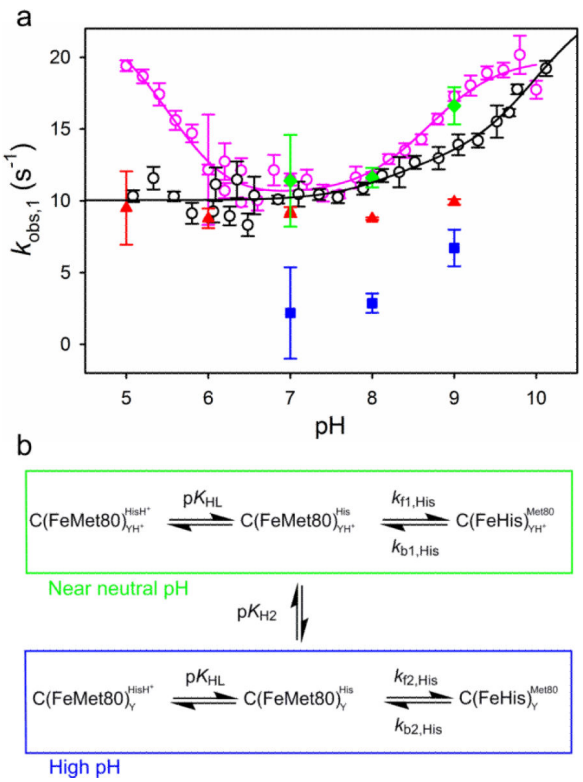

Fig. 6.

a Overlay of $k_{obs,1}$ vs pH from pH jump experiments for WT*/K73H (open black circles) and yWT/K73H (open pink circles, data are from ref. [30]) iso-1-Cyt*c*. All data were collected at 25 °C in 10 mM buffer containing 0.1 M NaCl. The black solid line is a fit of the WT*/K73H data to Eq. 3 from the Discussion and the pink solid line is a fit of the yWT/K73H data to Eq. 5 from ref. [30]. The microscopic rate constants, $k_{b,His}$ (red triangles) and $k_{f,His}$ (blue squares), extracted from gated ET experiments are shown for comparison. $k_{obs,1}$ (green diamonds) determined from gated ET experiments is also shown, where $k_{obs,1}$ is given by the sum of $k_{f,His}$ and $k_{b,His}$. **b** Kinetic scheme for the His73-mediated alkaline transition involving two ionizations used for the derivation of Eqs. 3 and 4 [23, 30]. The YH^+/Y ionization in the scheme corresponds to pK_{H2}.

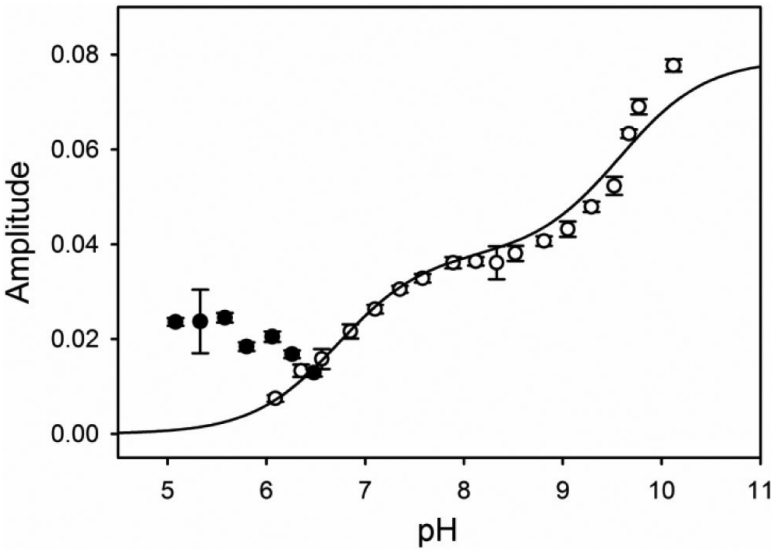

Fig. 7.

Amplitude versus pH for the fast phase ($k_{obs,1}$) from pH jump stopped-flow experiments. Amplitudes correspond to the change in absorbance at 406 nm. Upward (open circles) pH jump amplitudes are fit to Eq. 4 in the Discussion, derived from the kinetic scheme in Fig. 6b [23, 30]. The fit yields C_T equal to 0.164 ± 0.009. Downward pH jump amplitudes (filled black circles) are not used in the fit. Error bars on data points are the standard deviation of the average.

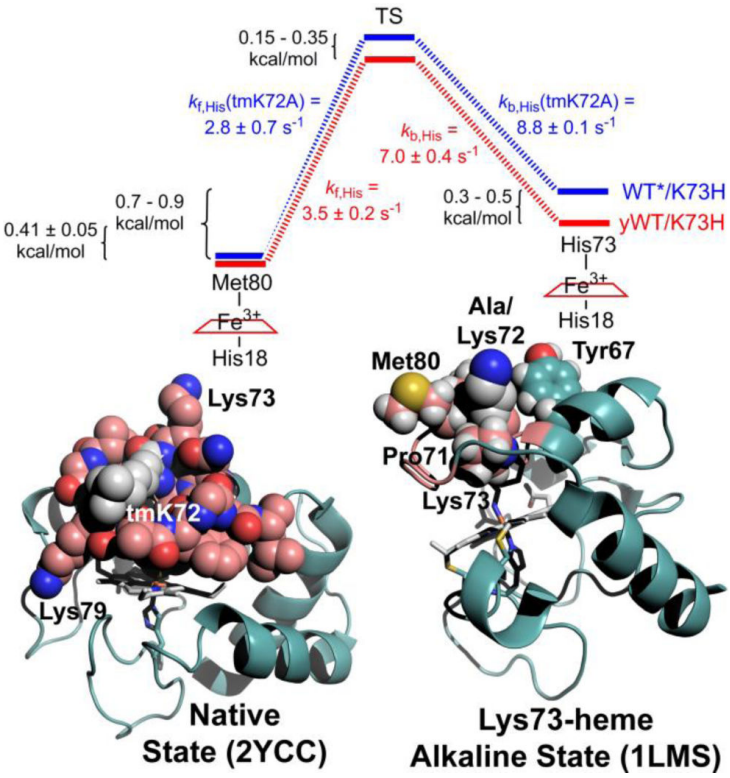

Fig. 8.

Effect of the tmK72A mutation on the free energy landscape of the His73-heme mediated alkaline conformational transition of iso-1-Cyt*c*. yWT/K73H has tmK72 and WT*/K73H carries the tmK72A mutation. The range given for the relative stabilities of the native conformer and His73-heme alkaline conformer for WT*/K73H is based on kinetic (0.7 kcal/mol; using $k_{f,His}$ and $k_{b,His}$ at pH 8 in Table 4 to obtained K_{C1}(His)) and thermodynamic data (0.9 kcal/mol, using pK_{C1}(His) in Table 2). The range in the magnitude of K_{C1}(His) produces a similar range for the relative stabilities of the His73-heme alkaline conformers of WT*/K73H and yWT/K73H. The change in the height of the barrier is calculated using the Eyring equation, yielding a decrease in the barrier for return to the native conformer by about 0.15 kcal/mol with the tmK72A mutation ($k_{b,His}$ increases from 7 to 8.8 s^{-1}). The range in the ΔG of the TS for WT*/K73H versus yWT/K73H results from the range in the ΔG of the His73-heme conformers of WT*/K73H and yWT/K73H. Lower left: structure of native iso-1-Cytc (pdb code: 2YCC with Ω-loop D colored salmon shown as a space-filling model. Lower right: structure of the Lys73-heme alkaline conformer (pdb code: 1LMS) with Ω-loop D colored salmon. Met80, Tyr67, Pro71 and Ala/Lys72 are shown as space filling models. Ala72 in this structure has been converted to Lys using the mutate function of PyMol (added carbons are shown in gray).

Table 1

Thermodynamic parameters for iso-1-Cyt*c* variants obtained by GdnHCl denaturation monitored by CD at 25 °C and pH 7.5.[a]

Variant	$\Delta G_u°'(H_2O)$ (kcal mol^{-1})	*m*-value (kcal mol^{-1}M^{-1})	C_m (M)
WT*	5.31 ± 0.08	4.39 ± 0.09	1.21 ± 0.01
yWT[b]	5.77 ± 0.40	5.11 ± 0.36	1.13 ± 0.02
WT*/K73H	4.09 ± 0.11	3.49 ± 0.12	1.17 ± 0.01
yWT/K73H[c]	4.32 ± 0.12	3.59 ± 0.01	1.20 ± 0.03

[a] Parameters are the average and standard deviation of a minimum of three trials.

[b] Parameters are from ref. [49].

[c] Parameters are from ref. [33].

Table 2

Thermodynamic parameters for the alkaline transition of iso-1-Cyt*c* variants obtained by pH titrations at 695 nm.[a]

Variant	pK_{C1}(His)	pK_{C2}(Lys)	pK_a(His)
WT*/K73H	0.67 ± 0.05	−2.04 ± 0.13	6.72 ± 0.10
yWT/K73H[b]	0.28 ± 0.01	−2.18 ± 0.11	6.60 ± 0.06
WT*/K79H[c]	−1.04 ± 0.04 (−1.06 ± 0.05)[d]	−2.8 ± 0.2	6.35 ± 0.04
yWT/K79H[e]	−0.99 ± 0.07 (−0.91 ± 0.03)[d]	−3.25 ± 0.24	6.62 ± 0.08

[a] Parameters are the average and standard deviation of a minimum of three trials

[b] Parameters are from ref. [20]

[c] Parameters are from ref. [27]. To fit equilibrium pH titration data more reliably, amplitude data from gated ET experiments were used to estimate the extinction coefficient of the native conformer

[d] Amplitude data from gated ET experiments at pH 7.5 were used to estimate pK_{C1}(His) [27]

[e] The extinction coefficient at 695 nm for fully native yWT/K79H was estimated using amplitudes from gated ET data reported in ref. [27] for yWT/K79H and used to refit equilibrium pH titration data for the yWT/K79H variant from ref. [23], as described in the Electronic supplementary material

Table 3

Rate and ionization constants for the His73-mediated alkaline transition of K73H variants of iso-1-Cytc at 25 °C in 10 mM buffer, 0.1 M NaCl

Parameter	Variant	
	WT*/K73H	yWT/K73H[a]
$k_{f1,His}$	3 ± 2	3.5 ± 0.2
$k_{b1,His}$	10.0 ± 0.2	7.0 ± 0.4
$k_{f2,His}$	12 ± 3	6.6 ± 0.2
$k_{b2,His}$	13 ± 9	13.2 ± 0.4
pK_{HL}	8.2 ± 0.6 (6.8 ± 0.1)[b]	6.4 ± 0.5
pK_{H2}	10.0 ± 0.6 (9.9 ± 0.2)[b]	8.7 ± 0.2

[a] Parameters are from ref. [30]

[b] Values in brackets are from fits of the two ionization mechanism to amplitude versus pH data.

Table 4

Rate constants obtained from reduction of oxidized WT*/K73H by hexaammineruthenium(II) chloride at 25 °C in 10 mM buffer, 0.1 M NaCl.[a]

pH	k_{ET} (mM^{-1}, s^{-1})[b]	$k_{b,His}$ (s^{-1})[c]	$k_{f,His}$ (s^{-1})[d]
5	44 ± 2	9 ± 2	-
6	47 ± 1	8.8 ± 0.7	-
7	42.4 ± 0.5	9.2 ± 0.4	2 ± 3
8	34.6 ± 0.7	8.76 ± 0.08	2.8 ± 0.7
9	31.6 ± 0.2	9.9 ± 0.2	7 ± 1

[a] Errors are standard errors reported by SigmaPlot unless otherwise noted

[b] k_{ET} is obtained from fits to Eq. 5, as described in the text. The intercepts, k_{uni}, of the fits to Eq. 5 were close to zero within error

[c] At pH 5 and 6, $k_{b,His73}$ is taken as the average value of $k_{gET,2}$ across all concentrations of a_6Ru^{2+}. Error is the standard deviation of the average. At pH 7 to 9, $k_{b,His}$ is from fits to Eq. 6, as described in the text

[d] From fits to Eq. 6, as described in the text